

# Shape resonances in photoionization cross sections and time delay

Anatoli S. Kheifets and Stephen Catsamas

<sup>1</sup>*Research School of Physics, The Australian National University, Canberra ACT 2601, Australia*

(Dated: November 30, 2022)

Shape resonances in photoionization of atoms and molecules arise from a particular geometry of the ionic potential which traps the receding photoelectron in a quasi-bound state in a particular partial wave. This mechanism allows us to connect the photoionization cross section in the resonant region with the photoelectron scattering phase in this partial wave by a simple formula  $\sigma \propto \sin^2 \delta_\ell$ . Due to this relation, the phase  $\delta_\ell$  can be extracted from an experimentally known cross section and then converted to the photoelectron group delay (Wigner time delay)  $\tau_W = \partial \delta_\ell / \partial E$  which is measurable by recently developed laser interferometric techniques. Such a direct connection of the photoionization cross section and the time delay is a fundamental property of shape resonances which provides a comprehensive test of novel measurements against a large body of older synchrotron data.

PACS numbers: 32.80.Rm 32.80.Fb 42.50.Hz

Shape resonances (SR's) affect profoundly numerous phenomena in physics, chemistry and biology (see Introduction of [1] for several fascinating examples). SR's have long been intensely studied in electron-molecule scattering [2] and molecular photoionization [3]. Similar resonant features are observed in electron-atom scattering [4] and atomic photoionization [5–7]. Formation of SR's is well understood [2–4, 8, 9]. SR's are associated with the shape of some effective potential in an open channel, normally a combination of short-range attractive and long-range repulsive potentials. Such a combination forms a barrier holding a large portion of the electron wave function while the remaining part of this wave function leaks out. This normally occurs at energies above and usually close to the threshold of that open channel and is typically associated with a large photoelectron angular momentum  $\ell \geq 2$ . A common property of SR's is that they can be turned into bound states by a slight modification of the target Hamiltonian [10, 11]. In molecules, SR's can be associated with anti-bonding vacant orbitals, typically of the  $\sigma^*$  character [12, 13].

A renewed interest in studying SR's has been promoted by recent development of laser interferometric techniques which allowed to resolve atomic and molecular photoionization in time. One such technique known as reconstruction of attosecond beating by interference of two-photon transitions (RABBITT) allowed to measure the photoelectron group delay in the SR region of various molecules:  $N_2$  [1, 14, 15],  $N_2O$  [16],  $CO_2$  [17],  $NO$  [18] and  $CF_4$  [19, 20]. A similar SR measurement in  $NO$  [21] was conducted using an attosecond angular streaking technique [22]. The photoelectron group delay, also known as the Wigner time delay, was introduced into particle scattering theory [23–25] and then extended to various applications including photoionization (see reviews [26–28]). In the presence of a SR, the photoelectron propagation is naturally delayed relative to the free space propagation. Thus the Wigner time delay acquires large positive values in the hundred of attoseconds range (1 as =  $10^{-18}$  s).

In general, an accurate determination of the Wigner

time delay requires detailed knowledge of elastic scattering phases and ionization amplitudes in various photoemission channels. Gaining knowledge of all these quantities amounts to performing a so-called complete photoemission experiment [29–31]. However, in a simple case of an isolated SR in a strongly dominant channel, the Wigner time delay can be expressed as the energy derivative of the photoelectron scattering phase in this particular channel  $\tau_W = \partial \delta_\ell / \partial E$ . In this Letter, we demonstrate that the phase in such a case can be extracted straightforwardly from the measured photoionization cross section. The latter is connected with the phase by a simple formula  $\sigma \propto \sin^2 \delta_\ell$ . We derive this relation from the integral equation relating the photoionization cross section with the transition  $T$ -matrix. The diagonal  $T$ -matrix allows to express the unitary scattering  $S$ -matrix and to find the elastic scattering phase. We examine several shape resonances in the  $nd \rightarrow \epsilon f, n = 3, 4$  ionization channels of the Xe atom and the  $I^-$  negative ion which demonstrate the  $\sigma(\delta)$  relation to a very high precision. Then we examine the SR in the NO molecule and find a consistency between the measured photoionization cross section [32] and the resonant Wigner time delay [30]. This way the experimental results obtained over a span of 30 years are seamlessly bridged. The SR analysis in the  $N_2$  molecule also supports our findings.

We start our derivation by expressing the photoionization amplitude as an integral of the dipole matrix with the transition  $T$ -matrix:

$$D_i(k) = d_i(k) + \sum_j \int p^2 dp d_j(p) G_{i,j}(p, k) T_{ij}(p, k). \quad (1)$$

Here the indices  $i, j$  describe the residual ion and  $p, k$  denotes the photoelectron momenta. The Green's function

$$G_{ij}(k, p) = (\epsilon_i + k^2 - \epsilon_j - p^2 - i\epsilon)^{-1}. \quad (2)$$

accounts for the energy non-conservation in the intermediate virtual state. We used Eq. (1) previously in convergent close-coupling calculations of multiple atomic photoionization [33, 34]. This equation is exhibited graphically in the top row of diagrams shown in Fig. 1. The

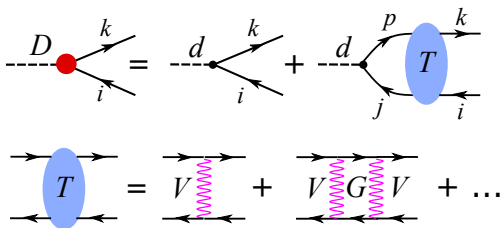


FIG. 1: Diagrammatic representation of the integrated dipole matrix element  $D(k)$  (top) and the scattering  $T$ -matrix (bottom). The following graphical symbols are in use: the straight line with an arrow to the right and left denotes a photoelectron and an ionic (hole) state, respectively. The dotted line exhibits a photon, the wavy line stands for the Coulomb interaction. The shaded circle and oval are used to represent the  $D$ - and  $T$ -matrices, respectively. The black dot stands for the bare dipole matrix element  $D(k)$ .

transition  $T$ -matrix is expressed via the Coulomb  $V$ -matrix by an infinite sequence of diagrams displayed in the bottom row of this figure. The knowledge of the  $T$ -matrix allows to express the unitary scattering  $S$ -matrix. In the case of a single-channel scattering, the said matrix is related to the elastic scattering phase [35]:

$$S(k) = e^{2i\delta(k)} = 1 - i2\pi k T(k, k) = 1 + 2\text{Im} G(k) T(k, k) \quad (3)$$

In the above expression, we dropped the single valued indices  $i, j$  defining the ionic state in the dominant scattering channel. The integral equation for the ionization amplitude (1) in a single channel approximation is reduced to

$$D(k) = d(k) + \int dp d(p)G(p)T(p, k) \quad (4)$$

$$\approx d(k)\text{Im} G(k) T(k, k) = \frac{1}{2} d(k) \left[ e^{2i\delta(k)} - 1 \right]$$

Here we assume that the integral term in the right-hand side of Eq. (4) is dominant over the bare term near the resonance and the Green's function can be represented by its on-shell imaginary part. Our numerical examples show that both assumptions are satisfied to a high accuracy near a SR. By squaring the modulus of the ionization amplitude (4) we arrive to the cross section

$$\sigma = \sigma_{\max} \sin^2 \delta(k) . \quad (5)$$

Here  $\sigma_{\max}$  is the cross-section maximum at the resonance which corresponds to  $\delta(k) = \pi/2$ . A similar expression is valid for the SR in the electron scattering

$$\sigma_{\ell}(k) = 4\pi k^{-2} (2\ell + 1) \sin^2 \delta_{\ell}(k) . \quad (6)$$

[11, 36]. The only difference is the normalization of the cross section to the incident electron flux rather than the cross-section maximum in Eq. (5).

In our numerical demonstrations of validity of Eq. (5), we use several approximations of reducing complexity.

The most accurate photoionization calculations account for inter-channel coupling between various atomic shells (inter-shell correlation). Such calculations are performed using the random phase approximation (RPA) [37]. In lesser accurate calculations, we switch off the inter-shell correlation and evaluate the ionization amplitude as a radial integral between the bound and continuum wave functions found in the Hartree-Fock (HF) approximation [38, 39]. By observing a close agreement between the RPA and HF photoionization cross sections we ensure the SR is indeed a single channel phenomenon. Finally, we evaluate the cross section from the elastic scattering phase  $\delta_{\ell}$  found in the HF approximation. For neutral atomic targets, we subtract the long-range Coulomb phase and use the phase difference  $\Delta_{\ell} = \delta_{\ell} - \sigma_{\ell}$ . It appears that the smooth Coulomb phase plays insignificant role in the SR formation.

We start our numerical demonstrations with the SR in the  $nd \rightarrow \varepsilon f, n = 3, 4$  ionization channels of the  $\Gamma^{-}$  negative ion. We use the ionic target to eliminate the long range Coulomb potential which would otherwise dominate the non-resonant Wigner time delay near the threshold. The top left panel of Fig. 2 displays the photoionization cross sections of the  $3d$  and  $4d$  shells of  $\Gamma^{-}$  calculated in HF the approximation as well as derived from the corresponding elastic scattering phases using Eq. (5). For comparison we display the RPA calculation for the whole  $4d$  shell cross-section correlated with the  $5s$  and  $5p$  shells. The relativistic RPA (RRPA) calculation for the  $4d$  shell [40] is also shown. We observe a close proximity of the RPA and HF cross sections which differ only marginally from the phase derived cross sections. The relativistic effects are also insignificant here. These observations support our assumption that the SR is largely a single-channel phenomenon and the cross section is derived mostly from the elastic scattering phase in a given partial wave. The bottom left panel of Fig. 2 displays the time delay in the  $nd \rightarrow \varepsilon f, n = 3, 4$  ionization channels. The two sets of differently styled curves exhibit the time delay in each channel as obtained by energy differentiation of the corresponding elastic scattering phase  $\tau(\delta)$  and as obtained from the photoionization cross section  $\tau(\sigma)$  using Eq. (5). The two methods of time delay determination produce very close results.

A similar data for Xe are presented in the right set of panels in Fig. 2. The calculated  $4d$  cross sections are compared with the experimental data [41, 42]. For the resonant time delay calculations, the effect of the Coulomb field is removed by using the reduced HF phases  $\Delta_{\ell} = \delta_{\ell} - \sigma_{\ell}$  where the analytically known Coulomb phases  $\sigma_{\ell}$  [43] are subtracted. Both the phase derived  $\tau(\Delta)$  and cross section derived  $\tau(\sigma)$  time delays are even closer in Xe than in the case of  $\Gamma^{-}$  as correlation effects are weakened in Xe by the Coulomb field of the ion remainder.

In both considered targets,  $\Gamma^{-}$  and Xe, the SR position depends very strongly on the depth of the  $nd$  hole. The Coulomb attractive potential acting on the depart-

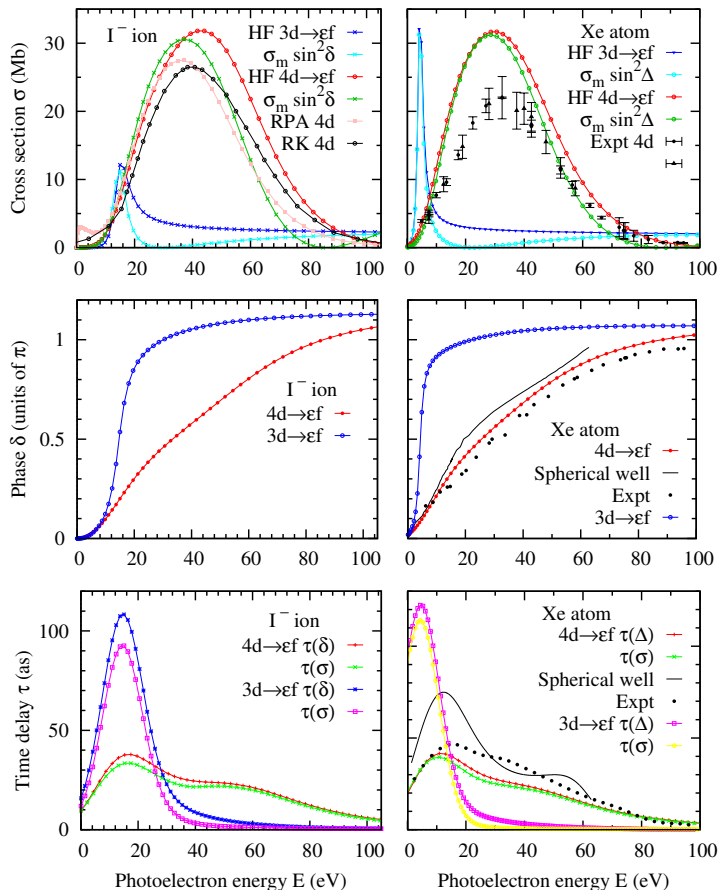


FIG. 2: Top: photoionization cross sections of the  $nd$  shells of  $I^-$  (left) and Xe (right). The HF cross sections in the dominant  $nd \rightarrow \varepsilon f$  channels are compared with the cross sections derived from the corresponding HF phases using Eq. (5). Also shown are the RPA calculation for the whole  $4d$  shell of  $I^-$  correlated with the  $5s$  and  $5p$  shells. A similar  $4d$  RRPA calculation by Radojević and Kelly [40] is marked RK. The  $4d$  cross section of Xe is compared with the experimental data [41, 42]. Bottom: time delay in the  $nd \rightarrow \varepsilon f$ ,  $n = 3, 4$  channels of  $I^-$  (left) and Xe (right) as calculated from the corresponding scattering phases and the photoionization cross sections. In Xe, the scattering phase and time delay are also derived from the experimental cross-sections (dots) and the spherical well model [7] (black solid lines).

ing photoelectron is stronger for a deeper  $3d$  hole which is screened less by outer atomic shells. Such an un-screened Coulomb potential counters the repulsive centrifugal potential more efficiently. As the result, the lower energy photoelectrons are trapped into the SR. This effect is somewhat stronger in the neutral Xe atom in comparison with the negative  $I^-$  ion. The photoelectron phase variation in the SR is close to one unit of  $\pi$ . When this variation occurs inside a narrow SR, the energy derivative of the phase and the corresponding Wigner time delay increase proportionally.

Connerade [36] applied a simple spherical well model to describe the SR in the  $4d$  photoionization of Xe and neighboring atoms. In this model, the photoelectron phase in the  $f$ -wave is expressed analytically via the spherical

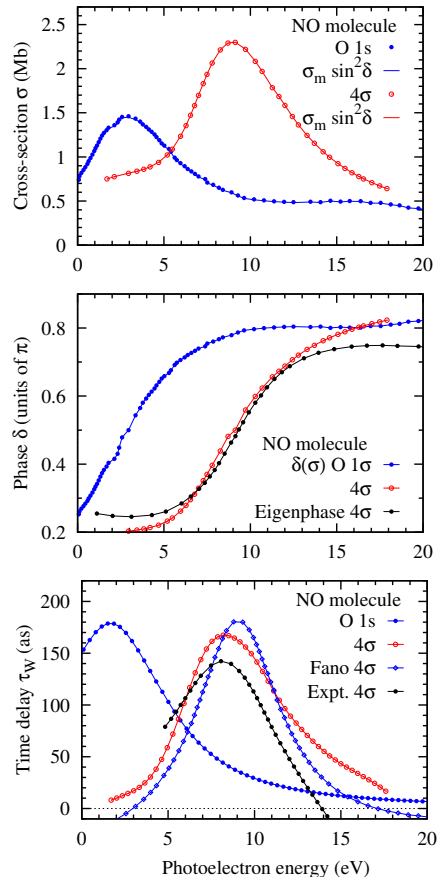


FIG. 3: Top: photoionization cross-sections of the core  $O 1s$  [32] and valence  $4\sigma$  [30] photoionization of NO. Middle: the photoelectron phases  $\delta(\sigma)$  derived from the cross-sections exhibited in the top pane. The  $4\sigma \rightarrow k\sigma$  eigenphase from [30] is shown for comparison. Bottom: the Wigner time delay  $\tau_W$  obtained by energy differentiation of the phases derived from the corresponding cross-sections. The  $\tau(\sigma)$  time delay is compared with the Fano formula delays calculated and measured in [30].

Bessel functions

$$\tan \delta_3 = \frac{z j_3(z') j_2(z) - z' j_3(z) j_2(z')}{z j_3(z') j_{-3}(z) + z' j_{-4}(z) j_2(z')}. \quad (7)$$

Here  $z = ak$  and  $z' = a\sqrt{k^2 + 2D}$  are functions of the photoelectron momentum  $k$ , depth  $D$  and radius  $a$  of the spherical potential well. Thus found phase  $\delta_3$  is fed into Eq. (6) with  $\ell = 3$  to find the cross-section which is displayed in the bottom panel of Fig. 1 of [36]. We retrofit this cross section with Eq. (6) and display thus extracted phase and time delay in the middle and bottom right panels of Fig. 2. The time delay in this model is markedly different from our calculations and the time delay obtained by feeding the experimental data [41, 42] into Eq. (5). More notably, the spherical well model fails completely for the SR in the  $3d$  photoionization. This indicates a much more complicated structure of this SR.

Next, we apply our analysis to the NO molecule. Here, the SR occurs because an unoccupied anti-bonding

$6\sigma(\sigma^*)$  orbital appears at a positive energy and merges with the  $k\sigma$  final state continua. In the meantime, an anti-bonding  $2\pi(\pi^*)$  orbital falls into the discrete spectrum and manifests itself as an isolated peak in the photoabsorption cross section. Due to this mechanism, the  $\sigma^*$  resonance is expected to be similar both in the core and valence shell ionization. We demonstrate this effect in Fig. 3 where we compare the oxygen  $1s$  [32] and the valence  $4\sigma$  [30] photoionization of NO. The corresponding photoionization cross-sections are displayed in the top panel of the figure. The absolute  $4\sigma$  photoionization cross-section is read from Fig. 1 of [30]. The relative O  $1s$  cross-section is read from Fig. 2 of [32] and scaled arbitrarily. In the middle panel of Fig. 3 we display the photoelectron scattering phases  $\delta(\sigma)$  extracted from the photoionization cross-sections exhibited in the top panel. For the valence  $4\sigma$  ionization, we make a comparison with the photoelectron scattering eigenphase exhibited in Fig. 5 of [30]. The latter phase is shifted vertically to match the cross-section derived phase. This shift does not affect the time delay which is expressed via the phase derivative. The phase comparison shows their rather similar slopes which are translated into similar time delays displayed in the bottom panel of Fig. 3. In the case of the valence  $4\sigma$  ionization, the time delay compares very closely with the Fano derived delays obtained from the calculated and measured data in [30]. These observations support the validity of the phase and time delay extraction from the corresponding photoionization cross-sections. We also observe a rather similar phase variation and time delay in the core and valence shell photoionization. This is in a sharp contrast to the atomic case illustrated in Fig. 2. Such a profound difference is explained by different mechanisms of the SR formation. In atoms, it is a competition of the attractive Coulomb and repulsive centrifugal potentials that leads to trapping the photoelectron in a SR. In molecules, it is the trapping the photoelectron into a vacant anti-bonding  $\sigma^*$  orbital which is rather insensitive to the photoelectron birth orbital. The only difference is an insignificant shift of the resonance energy which is marginal on the scale of the vastly different core and valence shell ionization potentials.

Finally, we derive the Wigner time delay from the cross-section of the valence  $3\sigma$  photoionization of the  $N_2$  molecule. Here the  $(3\sigma_g^{-1})X^2\Sigma_g^+$  channel contains a  $\sigma \rightarrow \sigma^*$  shape resonance merging with the  $3\sigma_g \rightarrow k\sigma_u$  continuum. For our analysis, we take the measured and calculated cross-sections displayed in Fig. 3B of [1] and re-plot them in the top frame of Fig. 4. There is an insignificant energy shift between the calculation and experiment due to the simplicity of the used theoretical model. The experimental data points are scattered and an analytic fit with Eq. (6) is applied to feed them, along with the calculated cross section, to Eq. (5). Thus derived phases are converted to the Wigner time delay by energy differentiation and the results are displayed in the bottom frame of Fig. 4. These results are compared

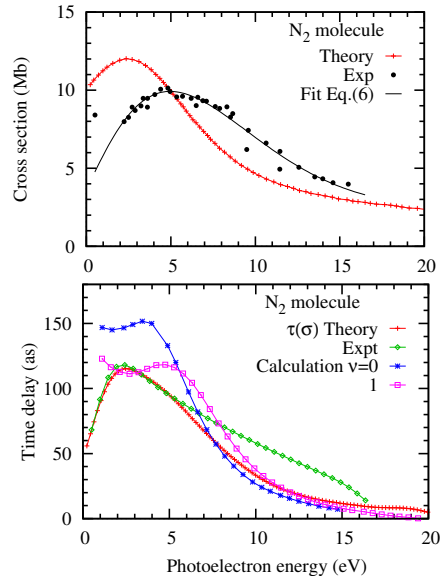


FIG. 4: Top: Photoionization cross-sections of the  $N_2$  molecule as calculated in [1] and measured in [44, 45]. The experimental cross section is fitted with the spherical well ansatz (6). Bottom: The time delay derived from the calculated and measured cross-sections are compared with direct calculations of [1] for the two lowest vibrational states  $\nu = 0, 1$  of the final  $X^2\Sigma_g^+$  ionic state.

with the time delays calculated in [1] for the two lowest vibrational states  $\nu = 0, 1$  of the final  $X^2\Sigma_g^+$  ionic state which contains the SR. While the fine details of the cross-section derived and directly calculated time delays differ, the overall shape and magnitude of both sets are quite similar.

In conclusion, we derive and test a fundamental relation between the cross section and the time delay in the region of a shape resonance in photoionization of atoms and molecules. While this relation is natural in electron scattering, it is demonstrated and rigorously proven in photoionization for the first time. This relation signifies an intimate link of photoionization and electron scattering processes which was demonstrated previously in multiple atomic photoionization [33, 34]. We support our findings by considering several examples of atomic SR's in the  $nd$  shells of Xe and  $I^-$  and molecular SR's in the  $n\sigma$  shells of  $N_2$  and NO. In the latter molecule, the SR in the core O  $1s$  photoionization is also considered. In the atomic cases, the  $\delta(\sigma)$  scattering phase produces the time delay which is almost identical with the directly calculated value. In molecules, small differences exist between the two sets but, generally, they agree remarkably well for such a simple model that we offer. The importance of the present findings is that they help to link a large data set of synchrotron measurements (see e.g. [46]) with the recent laser based interferometric experiments. This link offers a rigid test that allows to examine the consistency of the two sets of data. Another important observation is how the time delay varies when the depth of the atomic or molecular hole state changes. In atoms,

the time delay grows for inner shells in comparison with their valence counterparts. This finding supports the SR model in which the Coulomb field of the ionic core counterbalances the centrifugal potential in a large  $\ell$  partial wave. In molecules, another competing explanation is more relevant in which the SR occurs due to a trapping of

the photoelectron in a non-bonding vacant orbital. Such a trapping is rather insensitive to the birth place of the photoelectron.

*Acknowledgment:* The authors thank James Cryan and Taran Driver for many stimulating discussions.

- 
- [1] S. Nandi, E. Plésiat, S. Zhong, A. Palacios, D. Busto, M. Isinger, L. Neoricic, C. L. Arnold, R. J. Squibb, R. Feifel, et al., *Attosecond timing of electron emission from a molecular shape resonance*, *Science Advances* **6**(31), eaba7762 (2020).
- [2] J. N. Bardsley and F. Mandl, *Resonant scattering of electrons by molecules*, *Rep. Progr. Phys.* **31**(2), 471 (1968).
- [3] J. L. Dehmer, D. Dill, and A. C. Parr, *Shape resonances in molecular fields*, in *Fundamental Processes of Atomic Dynamics*, edited by J. S. Briggs, H. Kleinpoppen, and H. O. Lutz (Springer US, Boston, MA, 1988), pp. 541–563, URL [https://doi.org/10.1007/978-1-4684-5544-1\\_26](https://doi.org/10.1007/978-1-4684-5544-1_26).
- [4] I. Shimamura, *Quasi-bound states of electronic and positronic few-body systems*, in *Advances in Quantum Chemistry*, edited by C. A. Nicolaidis, E. Brändas, and J. R. Sabin (Academic Press, 2012), vol. 63 of *Advances in Quantum Chemistry*, pp. 165–245, URL <https://www.sciencedirect.com/science/article/pii/B978012397009100047>, et al., *Attosecond photoionisation time delays reveal the anisotropy of the molecular potential in the recoil frame*, *Nature Communications* **13**, 1242 (2022).
- [5] A. R. P. Rau and U. Fano, *Atomic potential wells and the periodic table*, *Phys. Rev.* **167**, 7 (1968).
- [6] U. Fano and J. W. Cooper, *Spectral distribution of atomic oscillator strengths*, *Rev. Mod. Phys.* **40**, 441 (1968).
- [7] J. P. Connerade, J. E. Esteve, and R. Karnatak, eds., *Giant Resonance in Atoms, Molecules and Solids* (Plenum, New York, 1986), no. 151 in *Nato Science Series B*.
- [8] T. A. Carlson, M. O. Krause, J. W. Taylor, P. R. Keller, M. N. Piancastelli, F. A. Grimm, and T. A. Whitley, *Recent developments in photoelectron dynamics using synchrotron radiation*, *IEEE Transactions on Nuclear Science* **30**(2), 1034 (1983).
- [9] M. Child, *Molecular Collision Theory*, *Dover Books on Chemistry Series* (Dover Publications, 1996).
- [10] M. Chrysos, *Simple spectral width estimation formula extracted from real energy shape resonance wavefunctions*, *J. Phys. B* **31**(7), 1391 (1998).
- [11] J. Horáček, *Resonance cross-section formula for low-energy elastic scattering*, *Phys. Rev. A* **100**, 032709 (2019).
- [12] P. W. Langhoff (American Chemical Society, 1984), vol. 263 of *ACS Symposium Series*, chap. *Molecular Photoionization Resonances. A Theoretical Chemist’s Perspective*, pp. 113–138.
- [13] M. Piancastelli, *The neverending story of shape resonances*, *J. Electr. Spectr. Relat. Phenom.* **100**(1), 167 (1999).
- [14] S. Haessler, B. Fabre, J. Higuët, J. Caillat, T. Ruchon, P. Breger, B. Carré, E. Constant, A. Maquet, E. Mével, et al., *Phase-resolved attosecond near-threshold photoionization of molecular nitrogen*, *Phys. Rev. A* **80**, 011404 (2009).
- [15] V. Loriot, A. Marciniak, S. Nandi, G. Karras, M. Hervé, E. Constant, E. Plésiat, A. Palacios, F. Martín, and F. Lépine, *Attosecond ionization time delay around a shape resonance in nitrogen measured by the RABBIT-2 $\omega$  method*, in *2021 Conference on Lasers and Electro-Optics Europe & European Quantum Electronics Conference (CLEO/Europe-EQEC)* (2021), pp. 1–1.
- [16] M. Huppert, I. Jordan, D. Baykusheva, A. von Conta, and H. J. Wörner, *Attosecond delays in molecular photoionization*, *Phys. Rev. Lett.* **117**, 093001 (2016).
- [17] A. Kamalov, A. L. Wang, P. H. Bucksbaum, D. J. Haxton, and J. P. Cryan, *Electron correlation effects in attosecond photoionization of CO<sub>2</sub>*, *Phys. Rev. A* **102**, 023118 (2020).
- [18] X. Gong, W. Jiang, J. Tong, J. Qiang, P. Lu, H. Ni, R. Lucchese, K. Ueda, and J. Wu, *Asymmetric attosecond photoionization in molecular shape resonance*, *Phys. Rev. X* **12**, 011002 (2022).
- [19] H. Ahmadi, E. Plésiat, M. Moiola, F. Frassetto, L. Poletto, P. Declève, C. D. Schröter, T. Pfeifer, R. Moshamb, et al., *Attosecond photoionisation time delays reveal the anisotropy of the molecular potential in the recoil frame*, *Nature Communications* **13**, 1242 (2022).
- [20] S. Heck, D. Baykusheva, M. Han, J.-B. Ji, C. Perry, X. Gong, and H. J. Wörner, *Attosecond interferometry of shape resonances in the recoil frame of CF<sub>4</sub>*, *Science Advances* **7**(49), eabj8121 (2021).
- [21] T. Driver, E. G. Champenois, J. P. Cryan, S. Li, A. Marinelli, P. Rosenberger, M. F. Kling, L. Ortmann, and A. Landsman, *Attosecond Electron Correlation and Molecular Resonance in K-shell Photoexcitation of Nitric Oxide* in *51st Annual Meeting of the APS Division of Atomic, Molecular and Optical Physics* (2020).
- [22] A. S. Kheifets, R. Wielian, V. V. Serov, I. A. Ivanov, A. L. Wang, A. Marinelli, and J. P. Cryan, *Ionization phase retrieval by angular streaking from random shots of XUV radiation*, *Phys. Rev. A* **106**, 033106 (2022).
- [23] L. Eisenbud, *Formal properties of nuclear collisions*, Ph.D. thesis, Princeton University (1948).
- [24] E. P. Wigner, *Lower limit for the energy derivative of the scattering phase shift*, *Phys. Rev.* **98**(1), 145 (1955).
- [25] F. T. Smith, *Lifetime matrix in collision theory*, *Phys. Rev.* **118**, 349 (1960).
- [26] C. A. A. de Carvalho and H. M. Nussenzveig, *Time delay*, *Phys. Rep.* **364**(2), 83 (2002).
- [27] P. C. Deshmukh and S. Banerjee, *Time delay in atomic and molecular collisions and photoionisation/photodetachment*, *Int. Rev. Phys. Chem.* **40**(1), 127 (2021).
- [28] P. C. Deshmukh, S. Banerjee, A. Mandal, and S. T. Manson, *Eisenbud-Wigner-Smith time delay in atom-laser interactions*, *Europ. Phys. J. Spec. Topics* **230**, 4151 (2021).
- [29] N. A. Cherepkov, G. Raseev, J. Adachi, Y. Hikosaka,

- K. Ito, S. Motoki, M. Sano, K. Soejima, and A. Yagishita, *K-shell photoionization of CO: II. determination of dipole matrix elements and phase differences*, J. Phys. B **33**(20), 4213 (2000).
- [30] F. Holzmeier, J. Joseph, J. C. Houver, M. Lebeck, D. Doweck, and R. R. Lucchese, *Influence of shape resonances on the angular dependence of molecular photoionization delays*, Nature Comms. **12**, 7343 (2021).
- [31] J. Rist, K. Klysssek, N. M. Novikovskiy, M. Kircher, I. Vela-Pérez, D. Trabert, S. Grundmann, D. Tsitsonis, J. Siebert, A. Geyer, et al., *Measuring the photoelectron emission delay in the molecular frame*, Nature Comms. **12**, 6657 (2021).
- [32] N. Kosugi, J. Adachi, E. Shigemasa, and A. Yagishita, *High-resolution and symmetry-resolved N and O K-edge absorption spectra of NO*, J. Chem. Phys. **97**(12), 8842 (1992).
- [33] I. Bray, D. V. Fursa, A. S. Kheifets, and A. T. Stelbovics, *Theory of electrons and photons colliding with atoms*, J. Phys. B **35**(16), R117 (2002).
- [34] I. Bray, D. Fursa, A. Kadyrov, A. Stelbovics, A. Kheifets, and A. Mukhamedzhanov, *Electron- and photon-impact atomic ionisation*, Physics Reports **520**(3), 135 (2012).
- [35] B. Bransden, *Atomic Collision Theory*, Lecture notes and supplements in physics (W. A. Benjamin, 1970).
- [36] J. P. Connerade, *A general formula for the profiles of 'giant resonances'*, J. Phys. B **17**(6), L165 (1984).
- [37] M. Y. Amusia, *Atomic photoeffect* (Plenum Press, New York, 1990).
- [38] L. V. Chernysheva, N. A. Cherepkov, and V. Radojevic, *Self-consistent field Hartree-Fock program for atoms*, Comp. Phys. Comm. **11**, 57 (1976).
- [39] L. V. Chernysheva, N. A. Cherepkov, and V. Radojevic, *Frozen core Hartree-Fock program for atomic discrete and continuous states*, Comp. Phys. Comm. **18**, 87 (1979).
- [40] V. Radojević and H. P. Kelly, *Photodetachment of the negative iodine ion including relaxation effects*, Phys. Rev. A **46**, 662 (1992).
- [41] B. Kammerling, H. Kossman, and V. Schmidt, *4d photoionisation in xenon: absolute partial cross section and relative strength of 4d many-electron processes*, J. Phys. B **22**(6), 841 (1989).
- [42] U. Becker et al, *Subshell photoionization of Xe between 40 and 1000 eV*, Phys. Rev. A **39**, 3902 (1989).
- [43] J. C. A. Barata, L. F. Canto, and M. S. Hussein, *New asymptotic formulae for the point Coulomb phase shift*, Brazilian J. Phys. **41**, 50 (2011).
- [44] A. Hammett, W. Stoll, and C. Brion, *Photoelectron branching ratios and partial ionization cross-sections for CO and N<sub>2</sub> in the energy range 18-50 eV*, J. Electr. Spectr. Relat. Phenom. **8**(5), 367 (1976).
- [45] E. W. Plummer, T. Gustafsson, W. Gudat, and D. E. Eastman, *Partial photoionization cross sections of N<sub>2</sub> and CO using synchrotron radiation*, Phys. Rev. A **15**, 2339 (1977).
- [46] J. W. Gallagher, C. E. Brion, J. A. R. Samson, and P. W. Langhoff, *Absolute cross sections for molecular photoabsorption, partial photoionization, and ionic photofragmentation processes*, J. Phys. Chem. Ref. Data **17**(1), 9 (1988).